Identification of regulators of germ layer morphogenesis using proteomics in zebrafish

Vinzenz Link, Lara Carvalho, Irinka Castanon, Petra Stockinger, Andrej Shevchenko and Carl-Philipp Heisenberg*

Max Planck Institute of Molecular Cell Biology and Genetics, Pfotenhauerstr.108, 01307 Dresden, Germany

*Author for correspondence (e-mail: Heisenberg@mpi-cbg.de)

Accepted 8 February 2006
Journal of Cell Science 119, 2073-2083 Published by The Company of Biologists 2006
doi:10.1242/jcs.02928

Summary

During vertebrate gastrulation, a well-orchestrated series of morphogenetic changes leads to the formation of the three germ layers: the ectoderm, mesoderm and endoderm. The analysis of gene expression patterns during gastrulation has been central to the identification of genes involved in germ layer formation. However, many proteins are regulated on a translational or post-translational level and are thus undetectable by gene expression analysis. Therefore, we developed a 2D-gel-based comparative proteomic approach to target proteins involved in germ layer morphogenesis during zebrafish gastrulation. Proteomes of ectodermal and mesendodermal progenitor cells were compared and 35 significantly regulated proteins were identified by mass spectrometry, including several proteins with predicted functions in cytoskeletal organization. A comparison of our proteomic results with data obtained in an accompanying microarray-based gene expression analysis revealed no significant overlap, confirming the complementary nature of proteomics and transcriptomics. The regulation of ezrin2, which was identified based on a reduction in spot intensity in mesendodermal cells, was independently validated. Furthermore, we show that ezrin2 is activated by phosphorylation in mesendodermal cells and is required for proper germ layer morphogenesis. We demonstrate the feasibility of proteomics in zebrafish, concluding that proteomics is a valuable tool for analysis of early development.

Supplementary material available online at
http://jcs.biologists.org/cgi/content/full/119/10/2073/DC1

Key words: Proteomics, Ezrin, Gastrulation, Zebrafish

Introduction

The systematic analysis of gene transcription patterns during development has been instrumental in the identification of a large number of candidate genes with potential functions in various developmental processes (reviewed by Stanford et al., 2001). By contrast, proteomic screens have very rarely been used to analyze developmental processes (Gong et al., 2004) despite indications that these approaches are complementary to large scale genomics (reviewed by Hebestreit, 2001; Lopez, 1999; Patton, 1999).

Proteomics may be a powerful method to study the downstream effects of signaling pathways on protein modifications. The identification of modifications regulating tissue morphogenesis during development currently poses a major challenge in developmental biology. The first morphogenetic process in the development of most multicellular organisms is gastrulation, during which a seemingly unstructured blastula transforms into a gastrula consisting of distinct germ layers (Stern, 2004). In zebrafish, gastrulation begins with the synchronized ingression of individual mesodermal and endodermal (mesendodermal) progenitor cells at the germ-ring margin, leading to the formation of a bi-layered embryo consisting of epiblast (ectodermal progenitors) and hypoblast (mesendodermal progenitors) (Montero et al., 2005; Warga and Kimmel, 1990). Ingression is followed by progenitor cells of both germ layers converging towards the dorsal side of the gastrula and redistributing along the anterior-posterior axis in a movement commonly named convergent extension (reviewed by Wallingford et al., 2002).

Various forward and reverse genetic approaches have provided insight into the genetic pathways controlling zebrafish germ layer formation (reviewed by Schier, 2001). TGF-β-like Nodal signals play a central role in this process by both inducing mesendodermal cell fates and controlling the cell-autonomous ingression of mesendodermal progenitors. In addition to Nodals, Wnt, PDGF and JAK/STAT signaling have all been shown to control different aspects of progenitor cell polarization and directed migration, although little is known about the precise molecular and cellular mechanisms by which these signaling pathways function during gastrulation (reviewed by Solnica-Krezel, 2005).

During germ layer formation, progenitor cells undergo pronounced changes in morphology and adhesion, suggesting that both cytoskeletal and cell adhesion proteins are crucial for this process. Wnt signals, for example, are thought to interfere with gastrulation movements by modulating the activity of adhesion molecules including cadherins (Puech et al., 2005; Torres et al., 1996; Ulrich et al., 2005) and by controlling cytoskeletal dynamics through activation of Rho kinase 2 (Rok2), a known regulator of actin-myosin contractility (Marlow et al., 2002). Interestingly, the immediate functions of

Wnts and other signals controlling gastrulation movements appear to be largely independent of changes in gene transcription (reviewed by Veeman et al., 2003), indicating that alternative mechanisms such as protein modifications are involved. However, no systematic approach has yet been undertaken to identify potential target proteins that are translationally regulated or post-translationally modified during gastrulation.

In this study, we have chosen a systematic comparative proteomic approach to identify proteins that are differentially expressed or modified between mesendodermal and ectodermal cells and might have essential roles for germ layer morphogenesis. We isolated 35 such proteins, four of which are likely to have functions in cytoskeletal organization. Comparison of our proteomic data with data obtained from an accompanying microarray-based gene expression screen revealed no significant correlation. This shows that we have identified proteins regulated on a translational or post-translational level that would not have been discovered by gene expression analysis. Finally, the functional analysis of one of the isolated proteins, ezrin2, revealed that ezrin2 is activated by phosphorylation in mesendodermal cells and is crucially required for germ layer morphogenesis during gastrulation. Our findings demonstrate that comparative proteomics in zebrafish represents an effective method to identify candidate proteins with important functions during early development.

Results

Proteomic analysis of ectodermal versus mesendodermal progenitor cells

To identify proteins involved in germ layer formation and morphogenesis, we performed a proteomic analysis of ectodermal versus mesendodermal progenitor cells (Fig. 1). We generated highly enriched pools of ectodermal and mesendodermal progenitor cells by overexpressing the Nodal signal Cyclops in wild-type embryos to obtain embryos primarily consisting of cells with mesendodermal character (Feldman et al., 2000) and using maternal zygotic *one-eyed-pinhead* (*oep*) mutant embryos as a source for ectodermal cells (Gritsman et al., 1999). We then compared the proteomes of ectodermal with mesendodermal cells taken from embryos at 7 hours post fertilization (hpf), as at this time in wild-type embryos, the first ectodermal and mesendodermal progenitor cells have already been sorted into their respective germ layers and ingression of mesendodermal progenitors is still ongoing.

We analyzed the samples by separating the proteins according to their molecular mass and isoelectric point (pI) on large-format two-dimensional (2D) gels, both, in the basic (pI 7-11) and acidic (pI 4-7) range (Fig. 2). We took advantage of the DIGE system for pre-separation fluorescent protein labeling with three separate dyes. To reduce gel-to-gel variability owing to lack of gel homogeneity, one dye was used as a common standard applied to all replicate gels. Spot matching, quantification and statistical analysis were carried out using 'Proteomweaver' software and significantly up- or downregulated spots were selected for subsequent analysis by mass spectrometry.

Comparison of ectodermal with mesendodermal cell extracts revealed 37 spots that significantly differed in their intensity on 2D gels (Table 1 and Table S1 in supplementary material). The large majority (31/37) of these were reduced in mesendodermal versus ectodermal cells. Using mass spectrometry, we were able to identify 36 out of 37 spots: four proteins have possible roles in the regulation of cytoskeletal dynamics, six proteins have less-defined but still potentially relevant functions for gastrulation (e.g. sialic acid synthase) and 25 proteins have metabolic or housekeeping functions. Two spots were identified as isoforms of the same protein.

Comparison of proteomic and genomic analysis

Microarray technology allows the quantitative analysis of gene expression on a genome-wide scale. To determine the overlap between comparative proteomics and gene expression profiling, we performed microarray analysis. The transcriptomes of ectodermal and mesendodermal cell populations, which were prepared with the same method as used for the proteomic screen, were analyzed on microarrays containing probes for more than 14,000 different zebrafish cDNAs (Affymetrix) (http://www.ebi.ac.uk/arrayexpress/query/entry, experiment accession number: E-MEXP-171). Based on a maximal FDR (false discovery rate) of 5% using the Benjamini-Hochberg algorithm (Benjamini and Hochberg, 1995), 220 genes showed significant regulation (Student's *t*-test: P_{max}=0.0004). Contrary to the results from our proteomic approach, more genes were upregulated (131) than downregulated (89) in mesendodermal versus ectodermal cells (Fig. 3A and Table S2 in supplementary material). To estimate on a gene-to-gene level the correlation of the proteomics data with the gene expression data, we compared the regulation factors of the 31 genes identified by proteomics which were represented on the microarray. Plotting the regulation factor on the protein level against the regulation factor on the RNA level

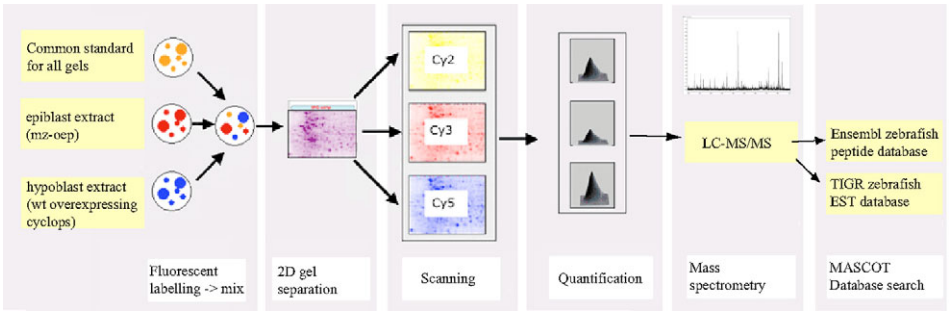

Fig. 1. Experimental layout. Ectodermal and mesendodermal protein extracts were labeled with Cy3 or Cy5 fluorescent dyes, combined and subsequently separated by 2D gel electrophoresis (DIGE). A common standard labeled with Cy2 was used for normalization. The scanned images were analyzed with Proteomweaver software to identify spots that displayed statistically significant changes. Differential spots were cut, digested with trypsin and analyzed by LC-MS/MS. Database searches were performed in Ensembl and TIGR databases using MASCOT.

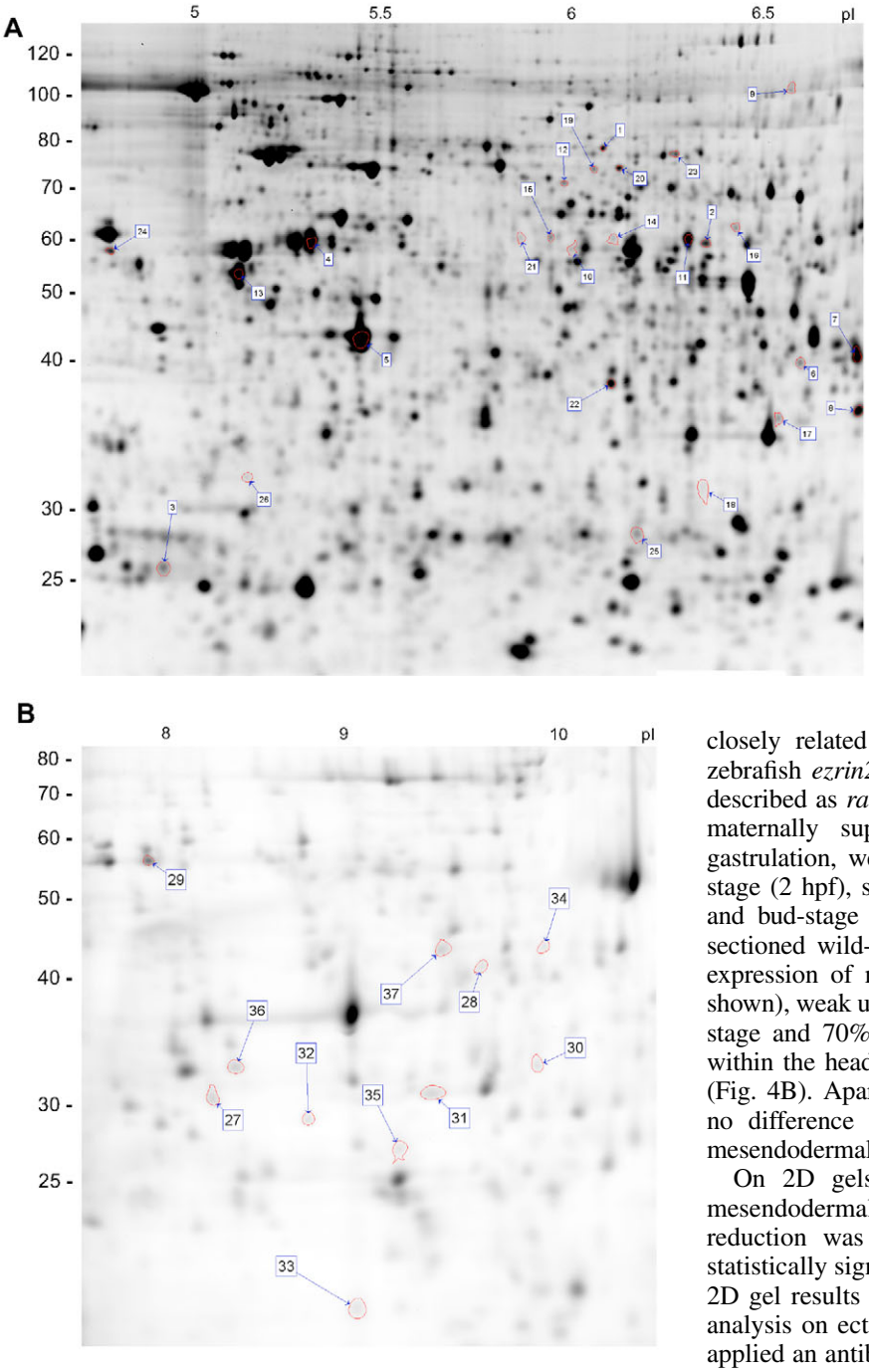

Fig. 2. 2D gel electrophoresis. Three Cy-dye labeled extracts (50 μg protein each) were combined and separated by 2D gel electrophoresis. First dimension: 24 cm strips pI 4-7 (A) and pI 7-11 (B). Second dimension, 25.5 × 20.5 cm 10% SDS polyacrylamide gels. Spots differentially regulated between ectodermal and mesendodermal cells are outlined in red, numbered and listed in Table 1.

revealed little correlation (Fig. 3B). Thus, the majority of the proteins identified by the proteomic approach were specifically regulated on a translational or post-translational level. This emphasizes the importance of comparative proteomics to identify protein modifications undetectable by gene expression profiling.

Regulation of ezrin2

One of the significantly regulated spots turned out to be a zebrafish ERM (ezrin, moesin, radixin) protein. Analyzing the phylogenetic relationship of this ERM protein to other known ezrin, moesin and radixin gene homologues in mouse, humans and *Drosophila* showed that the identified protein is most closely related to *ezrin* (Fig. 4A). We therefore termed it zebrafish *ezrin2* although the same gene has previously been described as *radixin* (see ZFIN rdx). To test whether *ezrin2* is maternally supplied and/or zygotically expressed during gastrulation, we performed in situ hybridizations on 32-cell-stage (2 hpf), shield-stage (6 hpf), 70% epiboly-stage (7 hpf) and bud-stage (10 hpf) embryos. In both whole-mount and sectioned wild-type embryos, we observed strong ubiquitous expression of maternal *ezrin2* at the 32-cell stage (data not shown), weak ubiquitous zygotic/maternal expression at shield-stage and 70% epiboly-stage, and strong zygotic expression within the head mesendoderm (prechordal plate) at bud stage (Fig. 4B). Apart from the expression in the prechordal plate, no difference in expression level between ectodermal and mesendodermal tissue could be detected (Fig. 4C).

On 2D gels, the ezrin2 spot was reduced 1.6-fold in mesendodermal cells as compared with ectodermal cells. This reduction was detected in all seven gels tested and was statistically significant ($P<0.0001$) (Fig. 5A,B). To confirm the 2D gel results independently, we performed western blotting analysis on ectodermal and mesendodermal cell extracts. We applied an antibody directed against a peptide fully conserved between human ERMs and zebrafish ezrin2 (ERM antibody). The antibody specifically detected two bands running very close to each other at about 78 and 80 kDa molecular mass, as reported for human ERM proteins, suggesting that it detects endogenous zebrafish ERM proteins (Fig. 5C). Comparing mesendodermal versus ectodermal cells, the signal was clearly decreased in the mesendodermal cells, confirming the regulation of ezrin2 previously observed on 2D gels.

ERM proteins are activated by phosphorylation of a conserved threonine at their C-terminus (Matsui et al., 1998), which can be specifically detected by an antibody directed against the phosphorylated site (phospho-ERM antibody). To obtain further insight into the regulation of ezrin2 during gastrulation, we tested whether ezrin2 is differentially

Table 1. Differentially regulated spots identified by mass spectrometry (top scoring hits are listed)

				2D Gel		Gene chip							
				Mesoderm/ectoderm		Mesoderm/ectoderm							
ID	Ensembl translation ID		Name	Regulation factor	*P* value (*t*-test)	Regulation factor	*P* value (*t*-test)	Score	Peptides	Sequence coverage	Molecular size (kDa)	pI
Cytoskeleton related												
1	ENSDARP00000047904		Ezrin2	0.64	0.0000	1.19	0.101	1801	38	46%	68	5.6
2	ENSDARP00000009161	MBRH HS	Fascin (Singed-like protein)	0.59	0.0000	3.41	0.002	1228	24	53%	55	6.1
4	ENSDARP00000004339	zfin	Tubulin, alpha 4 like	0.76	0.0001	0.70	0.025	1663	32	61%	51	5.0
5	ENSDARP00000000234	RHS MM	Actin, cytoplasmic 1 (Beta-actin)	0.78	0.0001	4.27	0.000	1029	20	69%	20	5.3
Others												
3	ENSDARP00000043647	family	14-3-3	0.39	0.0000	1.11	0.122	827	19	53%	28	4.7
7	ENSDARP00000024196	UBRH HS	Sialic acid synthase (N-acetylneuraminate synthase)	2.21	0.0000	1.35	0.010	555	13	46%	37	7.1
8	ENSDARP00000026638	UBRH MM	AU-rich element RNA-binding protein 1	0.76	0.0000	1.10	0.177	565	12	31%	34	6.9
9	ENSDARP00000013136	family	Iron responsive element binding 1	0.57	0.0009			372	11	20%	49	6.6
32	ENSDARP00000012822	UBRH HS	Calcyclin-binding protein (Siah-interacting protein)	0.73	0.0005	1.04	0.433	247	8	32%	26	8.7
35	TC237766	TIGR	NipSnap2 protein	0.67	0.0001	1.07	0.615	248	6	17%	38	9.2
Metabolic and housekeeping												
6	ENSDARP00000037059	UBRH HS	GDP-mannose pyrophosphorylase B isoform 1	1.87	0.0000	1.02	0.710	435	9	26%	41	6.4
10	ENSDARP00000039254	zfin	Aldehyde dehydrogenase 9 family, member A1	0.36	0.0000	0.80	0.015	649	15	30%	57	6.6
11	ENSDARP00000022715	zfin	Aldehyde dehydrogenase 9 family, member A1 like 1	0.50	0.0001	0.86	0.345	1622	31	70%	56	6.2
12	ENSDARP00000046666	UBRH HS	Asparaginyl-tRNA synthetase	0.54	0.0000	0.71	0.126	804	17	31%	58	5.4
13	ENSDARP00000031487	UBRH HS	ATP synthase beta chain	0.77	0.0001	1.43	0.008	2023	34	73%	55	5.1
14	ENSDARP00000021414	Vega	Similar to proteasome 26S subunit ATPase 1 (psmc1)	0.32	0.0000	0.80	0.021	1145	27	62%	49	6.0
15	ENSDARP00000030555	UBRH HS	26S protease regulatory subunit 4 (P26s4)	1.69	0.0001	0.87	0.124	563	15	29%	51	6.3
16	ENSDARP00000028600	UBRH HS	Delta 1-pyrroline-5-carboxylate synthetase	0.67	0.0000	0.89	0.508	723	15	21%	81	6.2
17	ENSDARP00000005850	UBRH HS	Delta-aminolevulinic acid dehydratase	0.36	0.0002	1.06	0.102	728	15	50%	35	7.5
18	ENSDARP00000024104	zfin	Carbonyl reductase 1-like	0.51	0.0011	0.74	0.002	239	4	19%	30	6.5
19	ENSDARP00000024219	family	XAA Pro Aminopeptidase 2 Precursor	0.22	0.0003	1.02	0.376	324	7	30%	25	5.4
20	ENSDARP00000028215	UBRH HS	Heat shock protein 75 kDa, mitochondrial precursor (HSP 75)	0.41	0.0000	0.88	0.543	941	17	39%	44	6.4
21	ENSDARP00000042383	MBRH HS	Heat shock cognate 71 kDa protein	0.53	0.0001	1.18	0.077	459	12	22%	71	5.3
22	ENSDARP00000004708	UBRH HS	NADH-ubiquinone oxidoreductase 42 kDa subunit, mitochondrial precursor	0.74	0.0000	1.18	0.015	986	21	55%	40	6.7
23	ENSDARP00000020266	UBRH HS	Propionyl-CoA carboxylase alpha chain, mitochondrial precursor	2.02	0.0000	1.19	0.054	1853	38	27%	68	6.6
24	ENSDARP00000048652	UBRH HS	Protein disulfide-isomerase precursor	0.69	0.0000			133	2	6%	41	4.9
25	ENSDARP00000042093	UBRH HS	S-methyl-5-thioadenosine phosphorylase	1.72	0.0000	0.70	0.012	931	21	49%	32	7.5
26	ENSDARP00000006133	UBRH HS	Ubiquitin thiolesterase protein OTUB1	0.24	0.0000			183	4	14%	31	4.9
27	ENSDARP00000050602	MBRH HS	Short chain 3-hydroxyacyl-CoA dehydrogenase, mitochondrial precursor	0.36	0.0000	0.47	0.002	393	9	23%	37	8.6
28	ENSDARP00000005028	UBRH HS	Fructose-bisphosphate aldolase B	0.33	0.0000	0.78	0.004	532	12	25%	37	8.3
29	ENSDARP00000027947	UBRH HS	ATP synthase alpha chain, mitochondrial precursor	0.63	0.0000			952	21	44%	42	9.4
30	ENSDARP00000006888		Not identified	0.59	0.0002							
31	ENSDARP00000014456	zfin	Voltage-dependent anion channel 2	0.69	0.0002	1.13	0.062	373	8	30%	30	8.8
33	ENSDARP00000023887	MBRH HS	NADH-ubiquinone oxidoreductase 19 kDa subunit	0.67	0.0001	1.12	0.096	168	4	20%	20	7.6
34	ENSDARP00000024560	UBRH GG	Aspartate aminotransferase, mitochondrial precursor	3.16	0.0000	1.68	0.000	321	6	21%	34	8.2
36	ENSDARP00000014912	Family	Delta 1-pyrroline-5-carboxylate reductase	0.70	0.0016	1.14	0.140	175	5	14%	32	6.7
37	ENSDARP00000024560	UBRH GG	Aspartate aminotransferase, mitochondrial precursor	0.37	0.0004	1.68	0.000	655	16	38%	34	8.2

See Table S3 in supplementary material for additional hits. Protein names are based on annotation by ZFIN or Vega or on Ensembl orthologue prediction. In the latter case, the result type of reciprocal BLAST analysis is provided alongside with the orthologue species (HS human, MM mouse, GG chicken). The average regulation factor together with the Student's *t*-test (two-sided, unpaired) is provided for the results of 2D gel and gene-chip analysis. ID 9, 24, 26 and 29 lack the gene-chip values because the corresponding gene was not represented on the chip. MOWSE-score was determined by MASCOT (1.8). Molecular mass and isoelectric point (pI) as predicted by Ensembl or TIGR.

phosphorylated between mesendodermal and ectodermal cells. Applying the phospho-ERM antibody, we detected increased levels of phosphorylated ERMs in mesendodermal versus ectodermal cells (Fig. 5C), indicating that ERMs, including ezrin2, are specifically phosphorylated in the mesendoderm. This regulation conflicts with the results obtained on the 2D gels and with the ERM antibody. It is likely that this inverse regulation observed with the ERM and phospho-ERM antibodies is due to specific detection of only unphosphorylated ERMs by the ERM antibody. This assumption is supported by the fact that the monoclonal ERM antibody we used in this study was raised against an unphosphorylated 11 amino acid peptide that is positioned at the threonine phosphorylation site. Consequently, phosphorylation of ezrin2 in mesendodermal cells would result in increased staining with the phospho-ERM antibody and decreased staining with the ERM antibody, as we have found. With respect to the observed regulation of ezrin2 on 2D gels, we speculate that the identified spot corresponds to the unphosphorylated form of ezrin2, which has been separated from its phosphorylated form as is often observed with protein phosphorylation on 2D gels.

To test for in vivo differences in ezrin expression or phosphorylation between the ectodermal and mesendodermal germ layers, we stained sections of gastrulating wild-type embryos with the ERM and phospho-ERM antibodies. Similar to our western blotting results, we found that mesendodermal progenitor cells, once ingressed at the germ ring margin, displayed elevated levels of phosphorylated ERM proteins on the cell membrane compared with adjacent non-ingressing ectodermal progenitor cells (Fig. 5D). Notably, phosphorylated ERM staining appeared rather variable both within the ectodermal and mesendodermal germ layers, indicating that

Fig. 3. Gene expression analysis. Gene expression changes between ectodermal and mesendodermal cells. Wild-type embryos consisting of both ectodermal and mesendodermal cells were compared with samples of ectodermal or mesendodermal cells using Affymetrix zebrafish gene arrays in triplicate. (A) The 220 most significantly regulated genes were selected based on an expected false discovery rate (FDR) of 5%. After centering and normalizing, the genes were clustered according to their regulation pattern. Color coding: up-regulated, red; unchanged, black; downregulated, green. (B) The regulation factor comparing mesendodermal with ectodermal cells on a transcriptional level was plotted against the regulation factor of 2D gel spot intensities. Areas of regulation in the same direction are shaded gray. The overall correlation between gene expression and spot intensity is weak.

ERM phosphorylation/dephosphorylation is dynamically regulated in these cells. In contrast to the phospho-ERM stainings, we only obtained weak, possibly nonspecific staining results using the ERM antibody, suggesting that this antibody, although working well on western blots, is not suitable for detecting ezrin2 expression in zebrafish tissue sections (data not shown).

Function of ezrin2

To analyze the function of ezrin2 during germ layer formation and morphogenesis, we knocked down *ezrin2* translation by injecting morpholino antisense oligonucleotides (MO) targeted against the translation initiation site of the *ezrin2* gene (*ezrin2* MO1; Fig. 6A). Injection of wild-type embryos with 4 and 8 ng of *ezrin2* MO1 led to a 1.4- and 2.2-fold reduction, respectively, of endogenous ezrin2 protein levels as determined on western blots (Fig. 6B), suggesting that the *ezrin2* MO1 effectively knocked down ezrin2 expression and that the ERM antibody detects ezrin2. This reduction in ezrin2 expression could be reversed by co-injecting 100-200 pg of a 5′-modified version of *ezrin2* mRNA, which does not bind the *ezrin2* MO1 (Fig. 6B).

ERM proteins are known to connect transmembrane proteins to the cytoskeleton (reviewed by Bretscher et al., 2002). Loss of function may therefore influence cell shape, adhesion and motility. Embryos injected with *ezrin2* MO1 showed reduced epiboly movements and in the most severe cases, the blastoderm completely detached from the yolk cell at early gastrulation (Fig. 7A). This phenotype appeared to be specific for *ezrin2* because we were able to both produce similar phenotypes using a second MO (MO2) targeted against the 5′UTR of *ezrin2* (Fig. 6A, Fig. 7C) and to rescue the *ezrin2* morphant phenotype by co-injection of *ezrin2* mRNA not targeted by the MOs (Fig. 6C). In addition, *ezrin2* morphant embryos displayed a shortened and broadened body axis at the end of gastrulation, indicating that convergent extension movements are affected (Fig. 7C,D). We found this phenotype in morphant embryos both before and after completion of epiboly, suggesting that reduced convergent extension is not just a secondary consequence of delayed development. By contrast, dorso-ventral patterning of early gastrula stage embryos was unaffected in *ezrin2* morphant embryos (data not shown).

To analyze the epiboly phenotype in more detail, we performed DIC microscopy of cells within the animal pole of late blastula/early gastrula stage embryos (4-5 hpf). Wild-type cells at the animal pole were typically organized into a compact assembly of round cells as seen by both DIC microscopy and phalloidin staining of cortical actin. By contrast, morphant blastodermal cells appeared more loosely associated and exhibited more spread-out and amorphic shapes (Fig. 7B). The degree of disorganization of cell shape and assembly correlated

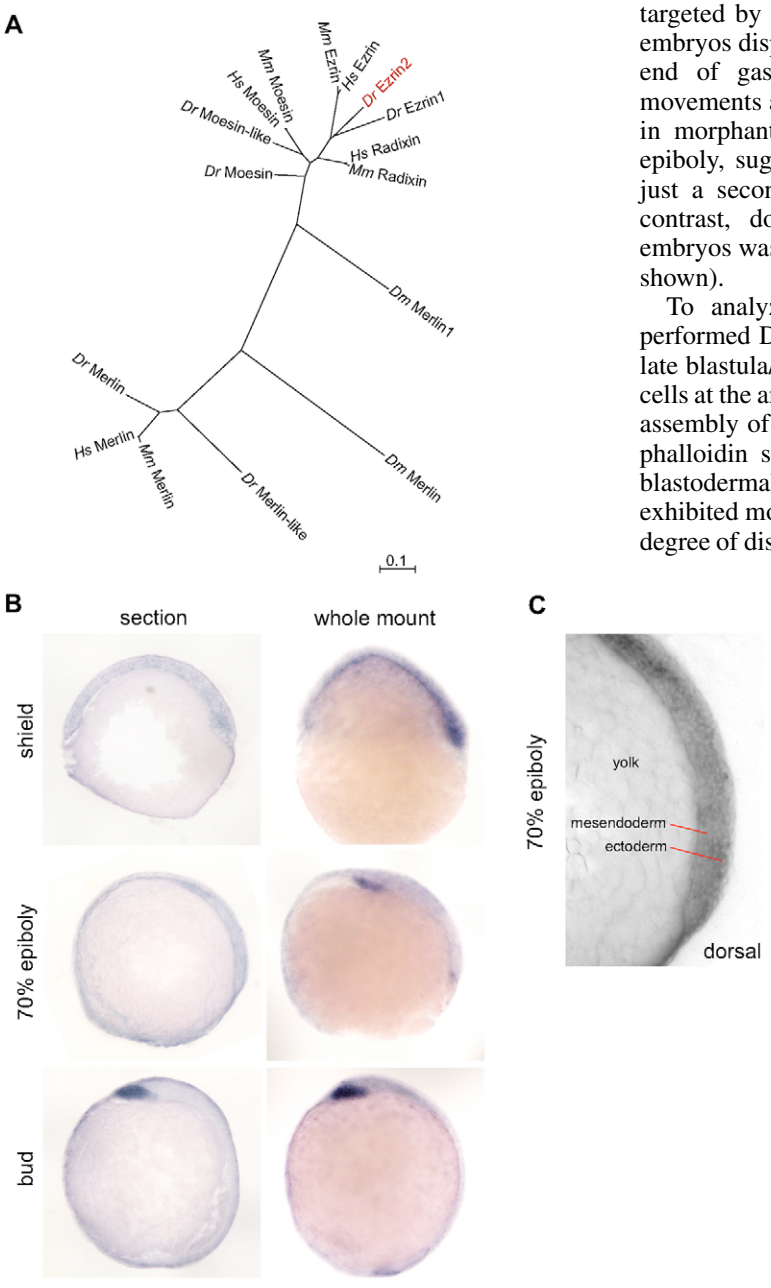

Fig. 4. Zebrafish ezrin2. (A) Un-rooted tree of human (*Hs*), mouse (*Mm*), zebrafish (*Dr*) and *Drosophila* (*Dm*) ERM-family proteins. Corresponding NCBI accession numbers: *Dr* Ezrin2 NP_001025456, *Hs* Ezrin NP_003370, *Mm* Ezrin P26040, *Dr* Ezrin1 XP_699992, *Hs* Radixin AAH47109, *Mm* Radixin NP_033067, *Mm* Moesin NP_034963, *Hs* Moesin P26038, *Dr* Moesin-like NP_001004296, *Dr* Moesin XP_700327, *Dm* Moesin P46150, *Dm* Merlin AAF49005, *Dr* Merlin-like NP_998116, *Mm* Merlin P46662, *Hs* Merlin P35240, *Dr* Merlin XP_689682. Scale bar indicates point mutations per site. (B) In situ hybridization of shield-stage (6 hpf), 70% epiboly-stage (7 hpf) and bud-stage (10 hpf) sectioned and whole-mount wild-type embryos using an *ezrin2*-antisense probe. Lateral views with dorsal side to the right. (C) Close-up view of the dorsal side of a sectioned 70% epiboly-stage (7 hpf) embryo after in situ hybridization using *ezrin2* antisense probe.

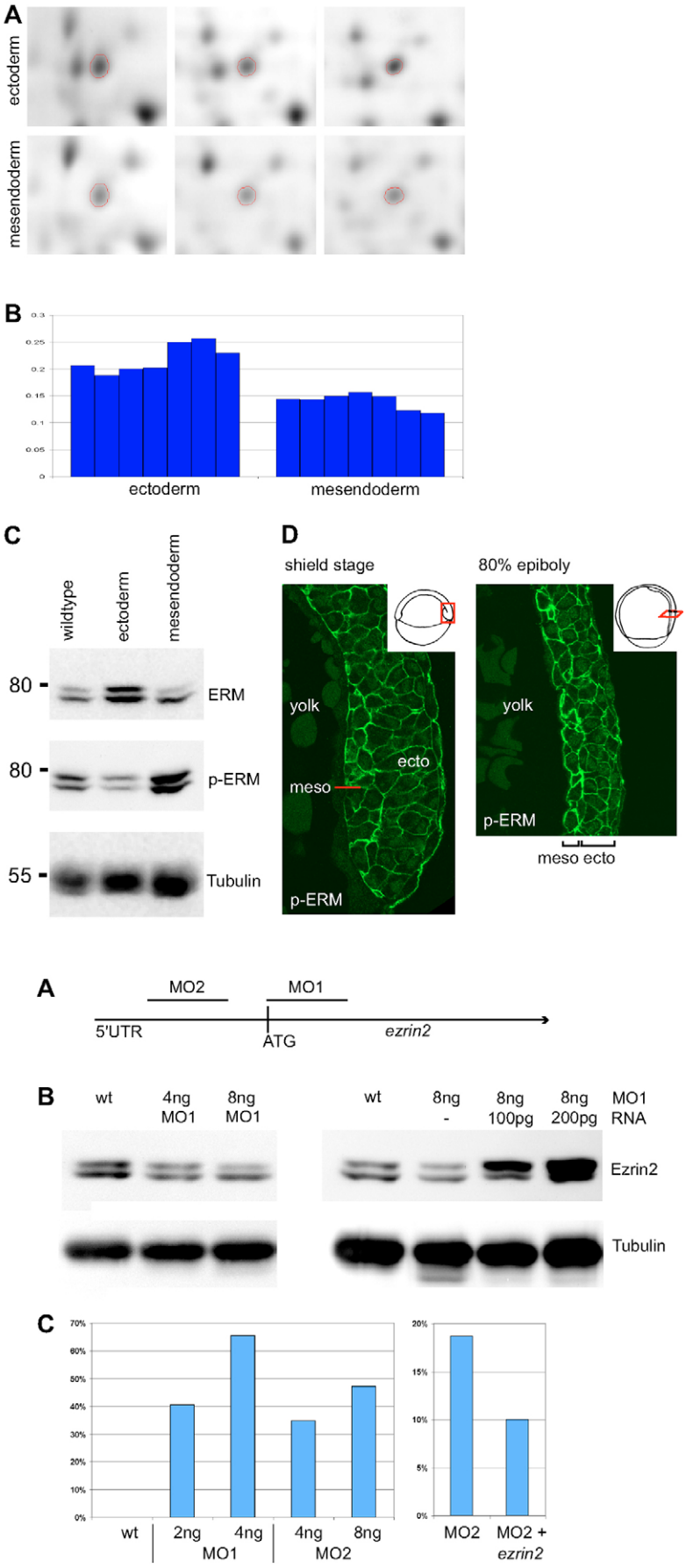

Fig. 5. Ezrin2 regulation analyzed by 2D gels, western blotting and immunostaining of sections. (A) Close-up view of three out of seven gels (Cy3 and Cy5 labeled) in the region of the ezrin2 spot (circled red). (B) Quantification of ezrin2 spot intensities of the DIGE 2D gel experiment. (C) Western blot analysis of wild-type, *mz-oep* (ectoderm) and *cyclops* mRNA injected (mesendoderm) embryos at 8 hpf (corresponding to 80% epiboly stage in wild-type embryos). After analysis with phospho-ERM (p-ERM) antibody, blots were stripped and re-probed with ERM antibody. The lower part of the blot was probed for tubulin as a loading control. (D) Wild-type embryos were sectioned at the shield stage (6 hpf; sagittal section through the shield region) and at 80% epiboly (8 hpf; transverse section through the emerging body axis, paraxial region) and stained with phospho-ERM (p-ERM) antibody. In mesendodermal cells the level of phosphorylated ERM proteins is increased. Insets show section planes.

Fig. 6. *Ezrin2* morpholino antisense oligonucleotides efficiently reduce ezrin2 protein level and impair gastrulation. (A) Placement of the *ezrin2* MOs used in this study (MO1 and MO2) on the *ezrin2* mRNA. MO1 targets the translation initiation site and MO2 is placed in the upstream 5′UTR of *ezrin2* mRNA. (B) Injection of *ezrin2* MO1 efficiently reduces ezrin2 protein as detected by western blotting with ERM antibody (tubulin antibody was used as loading control). Co-injection of 100 pg *ezrin2* mRNA with 8 ng of *ezrin2* MO1 restores ezrin2 protein expression. (C) Quantification of the early loss-of-function phenotypes and partial rescue by *ezrin2* mRNA injection. One-cell-stage embryos were injected with morpholino MO1 or MO2 and scored for blastoderm detachment or epiboly defects (wt 0/122, 2 ng MO1 37/91, 4 ng MO1 53/81, 4 ng MO2 38/109, 8 ng MO2 42/89). To rescue *ezrin2* morpholino-induced phenotypes 4 ng *ezrin2* MO2 followed by 100 pg *ezrin2* mRNA were injected. Embryos were scored for blastoderm detachment or epiboly defects (MO2 20/107; MO2 + *ezrin2* mRNA 9/90).

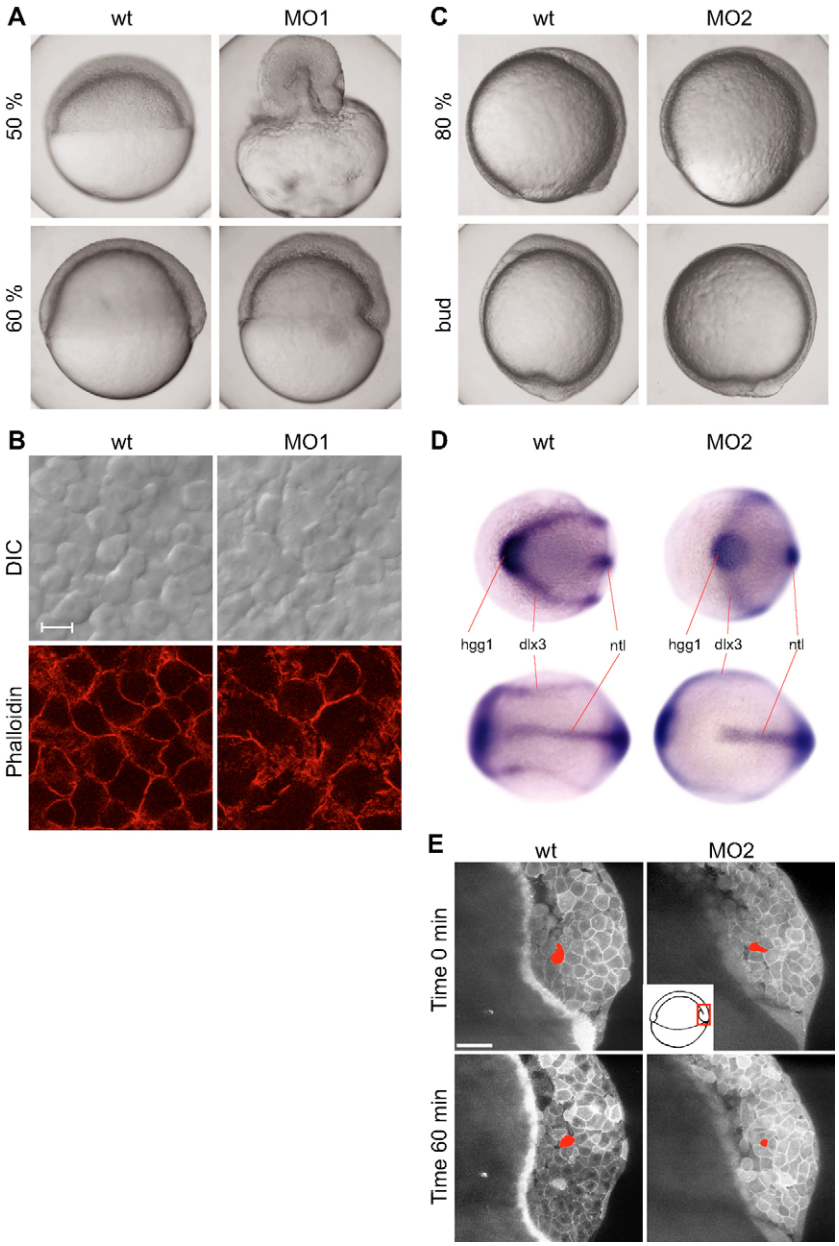

Fig. 7. Phenotypic characterization of ezrin2 morphant embryos. (A) Images of wild-type (wt) and *ezrin2*-MO1 injected embryos at 50% epiboly (5 hpf) and 60% epiboly (6 hpf). Dorsal side is to the right and the animal pole is up. (B) Face-on views of blastodermal cells within the animal pole of 50% epiboly (5 hpf) wild-type (wt) and *ezrin2* morphant (MO1) embryos as DIC images and stained for F-actin with phalloidin. Bar, 20 μm. (C) Images of wild-type (wt) and *ezrin2*-MO2 injected embryos at 80% epiboly (8 hpf) and bud stage (10 hpf). Dorsal side is to the right and the animal pole is up. (D) In situ hybridization of wild-type (wt) and *ezrin2*-MO2 injected embryos at the bud stage (10 hpf) with markers delineating convergent extension of the forming body axis. Upon morpholino injection, embryos developed a shortened notochord and a broadened neural plate. Animal views (upper panel) and dorsal views (lower panel), anterior to the left. Markers: notochord, *notail* (*ntl*); anterior edge of neural plate, *distal-less homeobox 3* (*dlx3*); prechordal plate, *hatching gland gene-1* (*hgg1*). (E) Analysis of cellular rearrangements within the axial germ ring (shield) of wild-type and *ezrin2* morphant embryos (MO2) starting at shield stage (6 hpf) by confocal time-lapse microscopy. Images correspond to timepoints 0 minutes and 60 minutes of Movies 1 and 2 in supplementary material. One exemplary mesendodermal progenitor cell was labeled in red to mark its position at 0 and 60 minutes of the time-lapse movie. Note that during this time interval the labeled cell has moved further away from the germ ring margin in the wild-type embryo compared with the morphant embryo, suggesting that mesendodermal cell migration is reduced within the shield of *ezrin2* morphant embryos. Lateral view, dorsal to the right. Bar, 40 μm.

with the strength of the epiboly phenotype. This suggests that, at the onset of zebrafish gastrulation, ezrin2 is required for the arrangement of blastodermal cells in compact cell assemblies needed for proper blastoderm epiboly.

The observation that in *ezrin2* morphant embryos, convergent extension movements are reduced at the end of gastrulation (Fig. 7C,D), together with the finding that ERM phosphorylation is increased in mesendodermal progenitor cells (Fig. 5C,D), suggests that ezrin2 phosphorylation and hence activation is required for proper mesendodermal progenitor cell migration. To obtain insight into the potential role of ezrin2 in this process, we recorded high-resolution two-photon confocal time-lapse movies of the cellular rearrangements within the axial germ ring margin (shield) of wild-type and *ezrin2* morphant embryos during the early stages of gastrulation. In wild-type embryos, mesendodermal progenitor cells, once delaminated, migrated as mesenchymal cells away from the germ ring margin towards the animal pole (Montero et al., 2005). By contrast, mesendodermal progenitors in morphant embryos were less motile and exhibited reduced animal-pole-directed migration (Fig. 7E and Movies 1 and 2 in supplementary material). This suggests that ezrin2, in addition to its earlier function in blastoderm epiboly, is required for proper mesendodermal progenitor cell migration.

Discussion

We have used comparative proteomics in zebrafish to identify proteins that are differentially expressed or modified in the embryonic mesendodermal and ectodermal germ layers and are therefore likely to be involved in morphogenesis of these tissues. Several proteins with presumed cytoskeletal functions were isolated as being regulated on a translational or post-translational level. One of these proteins, ezrin2, is activated

by phosphorylation in the mesendodermal cells and is required for proper germ layer morphogenesis during gastrulation. We conclude (1) that proteomics is feasible in zebrafish and (2) that comparative proteomics can be used to identify proteins that are specifically regulated on a translational or post-translational level and have essential functions during early development.

Gene expression profiles are usually compared by hybridizing microarrays that contain probes for a large number of cDNAs. In addition, large-scale enhancer, gene trap and in situ hybridization screens are performed to analyze the temporal and spatial pattern of gene expression. However, by comparing gene transcription only, potential differences due to translational or post-translational regulation of proteins cannot be detected. Comparative proteomics, by contrast, allows screening for differences on both translational and post-translational levels and therefore complements the transcriptional approaches. Although comparative proteomics is a powerful method, as demonstrated here, several technical limitations must be taken into account. First of all, despite remarkable advances of proteomic techniques in the last years, the dynamic range of this technology remains limited. Despite newly developed fluorescent dye techniques that allow quantitative analysis at nanogram levels, proteins of low abundance, which are estimated to compromise more than half the proteome, are commonly missed. Moreover, certain physicochemical properties such as hydrophobicity, molecular mass or isoelectric point can strongly decrease the recovery of specific proteins on 2D gels. Together, this ultimately narrows the range of proteins that can be identified using 2D-gel-based proteomics.

Although our proteomic approach did not cover the whole proteome owing to the intrinsic limitations of 2D gel technology, we were still able to quantitatively analyze more than 1000 different spots on our 2D gels. In addition to many proteins with metabolic or housekeeping functions, whose specific roles in germ layer morphogenesis are difficult to predict, we identified several regulatory and cytoskeleton-related proteins. Importantly, most of the genes identified by proteomics were not significantly regulated on a transcriptional level. Therefore, gene expression profiling alone would not have identified these genes.

It is noteworthy that, comparing mesendoderm and ectoderm, more of the significantly regulated spots were decreased than increased. This could be due to mesendoderm-specifying signals, such as Nodals, that modify proteins in epiblast (ectodermal) cells during their transition from epiblast into hypoblast (mesendodermal) cells. Considering that modifications increase protein heterogeneity, the resulting different protein isoforms in mesendodermal cells might fall below the detection limit as a result of their relatively low abundance. Consequently, the increase of these modified isoforms in mesendodermal cells might be undetectable whereas the decrease of the unmodified form is detectable.

Although most of the proteins identified here have not been investigated with regard to a specific function in development, previous studies suggest potential morphogenetic functions. For example, the small actin-bundling protein fascin is involved in the formation and regulation of cellular protrusions mediating motility, cell adhesion and cell interactions (reviewed by Adams, 2004), processes also involved in the regulation of gastrulation movements. Fascin activity is regulated by phosphorylation in response to signals from the extracellular matrix (ECM) or other external cues (reviewed by Kureishy et al., 2002). Furthermore, fascin expression in epithelial cell lines increased their 2D and 3D motility (Jawhari et al., 2003), again supporting the possibility that fascin has an important function in regulating cell movements during gastrulation. Another protein we identified here, sialic acid synthase, triggers the formation of sialic acids, which are terminal sugars on cell surface glycoproteins. Attachment of polysialic acid to the neural cell adhesion molecule (NCAM) serves to modulate cell interactions in the nervous system (Rutishauser and Landmesser, 1996). In addition, sialic acids serve as markers for cell-cell recognition events (reviewed by Varki, 1997). Sialic acids therefore may have the potential to influence gastrulation movements by modulating cell-cell adhesion and/or migration. Finally, 14-3-3 proteins have an extraordinarily widespread influence on cellular processes in all eukaryotes. They bind to phosphorylated-serine-containing peptides to regulate the activity and interactions of more than 200 proteins (reviewed by Mhawech, 2005). Interestingly, 14-3-3 proteins have also been reported to regulate cell migration and spreading by interactions with β_1 integrin, Raf and Cas (Rodriguez and Guan, 2005) and therefore are also likely to control cell migration during gastrulation.

Although we identified several regulatory and cytoskeleton-related proteins, we did not find any secreted/extracellular proteins or transcription factors, including those that previously have been identified as Nodal signaling targets (reviewed by Schier, 2003). Presumably, secreted proteins were lost during sample preparation because we dissociated the embryos during the de-yolking process, and transcription factors, which are generally known to be expressed at low levels, fell below the 2D detection limit.

Our experimental approach took advantage of the observations that Nodal signaling is both required and sufficient to induce mesendodermal cell fates in shield-stage embryos (reviewed by Schier, 2003). Although our assay was designed to reflect differential expression or modification between ectoderm and mesendoderm, we cannot exclude the detection of proteins targeted by Nodal signaling that is involved in other early developmental events such as left-right axis determination. Therefore, distribution and modification of every target protein must be independently analyzed in wild-type embryos to distinguish between direct Nodal targets and proteins regulated specifically in the mesoderm or ectoderm.

In this study, we have analyzed ezrin2 function during gastrulation. Ezrin2 belongs to the family of closely related ERM proteins (Sato et al., 1992) that link filamentous actin to integral plasma membrane proteins upon phosphorylation mediated activation (Matsui et al., 1998), thereby regulating cell shape, surface structures, adhesion and motility. Furthermore, ERMs have been implicated in signal transduction regulation by altering membrane protein localization and internalization (reviewed by Bretscher et al., 2002). Studies in cell culture have suggested that ezrin is concentrated at the leading edge of migrating cells and that blocking ezrin function leads to defective extension of pseudopods and collapse of the leading edge (Crepaldi et al., 1997; Lamb et al., 1997). Our finding that in ingressing mesendodermal progenitors, ezrin2 gets phosphorylated and

hence activated, suggests that ezrin2 activity is involved in mesendodermal cell ingression and subsequent migration. Evidence for a crucial role of ezrin2 in the forming mesendoderm came also from our morpholino-based loss-of-function analysis, which showed that proper mesendodermal progenitor migration depends on normal ezrin2 expression.

In addition to the mesendodermal phenotype in *ezrin2* morphant embryos, we observed distortions of cell shape and assembly within the blastoderm of pre-gastrula-stage embryos, followed by reduced epiboly movements and, in the most severe cases, complete delamination of the blastoderm from the yolk cell. Ezrin has previously been shown to interfere with compaction and cavitation of the blastocyst in pre-implantation mouse embryos (Dard et al., 2001), suggesting a similar function in regulating blastoderm cell compaction in zebrafish and mouse. Future studies will have to elucidate the molecular and cellular mechanisms by which ezrin functions in cell compaction and how this function is related to its effects on epiboly and convergent extension movements during gastrulation.

In conclusion, we have demonstrated that proteomics can be used in zebrafish to identify proteins that are regulated on a translational or post-translational level. Further characterization of one of the identified proteins, ezrin2, revealed that ezrin2 is phosphorylated in mesendodermal cells and required for proper germ layer morphogenesis during gastrulation. Proteomics can therefore be used to identify proteins with essential functions during zebrafish gastrulation.

Materials and Methods

Embryo maintenance

All wild-type embryos were obtained from zebrafish TL, AB and Golden lines. Fish maintenance and embryo collection was carried out as described (Mullins et al., 1994). Embryos were staged as previously described, grown at 31°C and manipulated in E3 zebrafish embryo media (Kimmel et al., 1995).

Sample preparation

To obtain mesendodermal progenitor cells, wild-type embryos were injected with 100 pg *cyclops* mRNA. Ectodermal progenitor cells were obtained from maternal-zygotic *one-eyed-pinhead* (*oep*) mutant embryos (Gritsman et al., 1999). The embryos were dechorionated and deyolked with two extra washing steps as previously described (Link et al., 2006).

DIGE labeling and 2D gel electrophoresis

20 μl lysis buffer (7 M urea, 2 M thiourea, 4% Chaps, 30 mM Tris-HCl pH 9.2) was added to the cells of 100 de-yolked embryos. The sample was incubated shaking for 15 minutes at 8°C after the addition of 0.5 μl benzonase (25 U/μl, >99% purity, Novagen) to degrade DNA/RNA. Protein concentration was determined by RC DC Protein assay (Bio-Rad). Insoluble particles were removed by centrifugation for 1 hour at 60,000 ***g***. 50 μg protein was then labeled with 200 pmol Cy dye as described in the user manual (Amersham Biosciences). The samples labeled with different dyes were combined. For 2D gels of proteins in the acidic range (pI 4-7), labeled samples were mixed with 450 μl rehydration solution (pI 4-7: 7 M urea, 2 M thiourea, 4% Chaps, 5% isopropanol, 2.5% glycerol, 1% DTT, 5 μl/ml Bio-Lytes 3/10 (Bio-Rad) and 450 μl of this solution was applied to a 24 cm strip (pI 4-7, Amersham Biosciences) for rehydration loading overnight. The focusing conditions for Protean IEF cell (Bio-Rad) were 30 minutes linear 0 V to 150 V, 1.5 hours 150 V, 1 hours 250 V, 4 hours linear 250 V to 1000 V, 1.5 hours linear 1000 V to 5000 V, 2 hours linear 5000 V to 10,000 V, 10,000 V for 80 kVhours, 500 V until proceeding to second dimension. For 2D gels of proteins in the basic range (pI 7-11), labeled samples were brought to 10 mM DTT and 5 μl/ml IPG buffer pH 6-11 (Amersham Biosciences). Strips (pI 7-11, Amersham Biosciences) were rehydrated overnight with 450 μl rehydration solution (7 M urea, 2 M thiourea, 0.5% Chaps, 12 μl/ml Destreak (Amersham Biosciences), 5 μl/ml IPG buffer (pH 6-11). The sample was applied by cup-loading at the anodic side. The focusing conditions for Protean IEF cell (Bio-Rad) were 1 hour linear 0 V to 150 V, 1 hour 150 V, 3 hours 300 V, 2 hours 500 V, 3 hours linear 500 V to 1000 V, 5 hours linear 1000 V to 10,000 V, 10,000 V for 50 kVhours, 500 V till proceeding to second dimension. As protease inhibitors, we added to all buffers before the first dimension a mix of 1 mM EDTA, 10 μM E64c, 0.002 mg/ml aprotinin and 1 μM pepstatin A. Focused strips were reduced (15 minutes 20 mg/ml DTT) and alkylated (15 minutes 25 mg/ml IAA) in equilibration buffer (50 mM Tris-HCl pH 8.8, 6 M urea, 30% glycerol, 2% SDS, 0.002% Bromophenol Blue), loaded on 10% SDS-polyacrylamide gels and run on Ettan Daltsix (Amersham Biosciences) (2 hours 8 mA/gel, 16 hours 85 V). Gels were scanned with Typhoon 9410 Variable Mode Imager (Amersham Biosciences).

Quantification

A mixture of mesendodermal and ectodermal samples was labeled with Cy2 and used as internal standard for all replicate gels. The experiment was performed in triplicate and every sample was analyzed once Cy3 and once Cy5 labeled. Spot detection, matching and quantification were performed using Proteomweaver 3.0 software (Definiens, Munich, Germany).

Mass spectrometry

Gels were stained with colloidal Coomassie Blue (Kang et al., 2002) for visual detection of spots. Spots were manually excised, reduced, alkylated and in-gel digested with trypsin as previously described (Shevchenko et al., 1996). Extracted peptides were dried in a vacuum centrifuge and subsequently redissolved in 10 μl of 0.04% trifluoroacetic acid (TFA).

Samples were analyzed by LC-MS/MS with LTQ ion trap mass spectrometer (Thermo Electron, San Jose, CA) coupled to UltiMate Plus nano LC system (LC Packings, Amsterdam, The Netherlands). 4 μl of the sample was injected and separated by reverse-phase HPLC (C18 PepMAP100, ID 75 μm, length 15 cm; LC Packings) with mobile phases of 0.1% formic acid (A) and 80% acetonitrile (B) for 20 minutes 0-20% B, 15 minutes 20-50% B and 5 minutes 50-100% B. The mass spectrometer was operated in data-dependent mode alternating between MS and MS/MS on the five most abundant peaks using dynamic exclusion. Database search was performed using MASCOT (1.8, Matrix Science LTD, U.K.) against the TIGR zebrafish gene index (ftp://ftp.tigr.org/pub/data/tgi/Danio_rerio/ZGI.release_16.zip) and the Ensembl zebrafish peptide database (http://www.ensembl.org/info/data/download.html zebrafish->peptide->*.fa.gz). MASCOT search parameters were peptide precursor mass tolerance, ±2 Da; mass tolerance fragment ions, ±0.5 Da; enzyme specificity, trypsin; missed cleavages tolerated, 1; fixed modifications, carbamidomethyl; no variable modifications.

Microarray analysis

RNA was extracted from de-yolked cells using NucleoSpin RNA II kit (protocol 5.1, Macherey-Nagel, Dueren, Germany). RNA was then precipitated with sodium acetate pH 5.2, washed twice with 80% ethanol and re-suspended to a concentration of 1 μg/μl. ServiceXS (Leiden, The Netherlands) performed the labeling and hybridization experiments using MessageAMPII kit (Ambion, Austin TX, USA) and Affymetrix Zebrafish Genome arrays (Affymetrix, Santa Clara CA, USA). Statistical analysis was performed with ArrayAssist software (Stratagene, La Jolla CA, USA). The raw data (CEL-format) was processed by PLIER (www.affymetrix.com) probe level analysis and logarithmic transformation. Three independent replicates of each condition were analyzed. Student's *t*-test was applied with a maximal FDR (false discovery rate) of 5% (Benjamini-Hochberg algorithm). Significantly regulated genes were centered, normalized and then hierarchically clustered with 'Cluster 3.0' software (Eisen et al., 1998). Fig. 3A was generated with 'Gene Treeview'.

Phylogenetic tree

Sequences fetched from NCBI were aligned using Clustal X (Thompson et al., 1997). The tree was generated with PHYLIP (Felsenstein, 1989), distancematrix protdist, 100 iterations calculated using the fitch algorithm.

Western blotting

De-yolked samples were dissolved in 2 μl 2× SDS sample buffer per embryo and incubated for 5 minutes at 95°C and loaded on SDS gels. Electrophoresis, blotting and detection was performed as previously described (Link et al., 2006). Before re-probing, membranes were incubated for 30 minutes at 50°C in stripping solution (100 mM 2-mercaptoethanol, 2% SDS, 62.5 mM Tris-HCl pH 6.7) followed by two washes for 5 minutes each with PBST. Antibodies used were anti-MEK1/2 (Cell Signaling #9122, 1:1000), anti-α-tubulin (Sigma T6199, 1:2000), anti-ERM (BD Biosciences 610401, 1:1000) and anti-phosphorylated-ERM (Cell Signaling #3141, 1:1000).

Morpholino oligonucleotide and mRNA injection

For MO injections the following MOs directed against zebrafish ezrin2 were injected into one-cell-stage embryos: (MO1 directed against the 5′ coding sequence) 5′-CGCGAACATTTACTGGTTTAGGCAT-3′ and (MO2 directed against the 5′UTR) 5′-GATGTAGATGCCGATTCCTCTCGTC-3′ (Gene Tools, Philomath, OR). MOs were designed according to Gene Tools targeting guidelines. MO sequences were then compared with the Ensembl database by using BLAST, and no significant similarities were found to any sequences other than zebrafish *ezrin2*. For mRNA injection, *ezrin2* full-length cDNA was cloned by PCR into pCS2^{+} vector. Seven mutations changing two valines to isoleucines were introduced at the MO1 binding site (ATGCCTAAACCAa(G)Tc(A)AAc(T)a(G)Tc(T)a(C)Ga(C)-GTC) so that MO1 could not bind the injected mRNA. mRNA was transcribed from

pCS2-*ezrin2* by using the SP6 mMessage mMachine (Ambion, Austin, TX) and injected into one-cell-stage embryos.

In situ hybridization and sectioning

Whole-mount in situ hybridization was performed as previously described (Barth and Wilson, 1995). For *ezrin2*, sense and antisense RNA probes were synthesized from the *ezrin2* full-length cDNA. For *hgg1*, *ntl* and *dlx3* in situ hybridization, antisense RNA probes were synthesized from partial sequences of the respective cDNAs. For sectioning, in situ-stained embryos were equilibrated in gelatine/albumin solution (0.49% gelatine, 30% egg albumin, 20% sucrose in PBS), transferred into fresh polymerization solution (25% glutaraldehyde in gelatin/albumin solution, 1:10) and polymerized for 15 minutes at room temperature. 40 μm serial sections were taken using a Leica Vibratome VT1000S.

Immunostaining of sectioned embryos

Embryos were fixed in 4% paraformaldehyde overnight at 4°C, dehydrated and embedded in paraffin wax. 10 μm serial sections were taken on a microtome, dried overnight at 37°C and then rehydrated. Immunostaining was done according to manufacturer's instructions for the anti-phosphorylated-ERM antibody (phospho-ERM) (Cell Signaling #3141). Briefly, for antigen retrieval, the slides were boiled in 10 mM sodium citrate buffer pH 6.0 and kept at sub-boiling temperature for 10 minutes. Samples were washed with TBST (Tris-buffered saline, 1% Tween-20) and blocked with 5% normal goat serum in TBST for 2 hours at room temperature. Then, they were incubated overnight at 4°C with phospho-ERM antibody 1:25 in blocking solution, followed by several washes with TBST and incubation with secondary antibody (Alexa Fluor 488 anti-rabbit 1:1000; Invitrogen), for 2 hours at room temperature. After several washing steps, sections were mounted in DABCO medium and images were acquired with a Leica TCS SP2 confocal microscope.

Image acquisition and quantification

DIC images were taken as previously described (Montero et al., 2003). For F-actin phalloidin staining, the embryos were fixed in 4% paraformaldehyde overnight at 4°C, permeabilized for 4-5 hours in PBST, incubated for 1 hour in Rhodamine-conjugated phalloidin (1:200; Invitrogen) and then rinsed several times in PBST. Stained embryos were mounted on agarose-coated dishes in PBST medium with the animal pole facing up, and images were acquired with a Leica TCS SP2 confocal microscope. To record confocal time-lapse movies, we injected a mixture of 90 pg GAP43-eGFP mRNA and 30 pg GFP mRNA into one-cell-stage embryos. The movies were recorded as previously described (Montero et al., 2005) using a BioRad Radiance 2000 multiphoton confocal microscope with a 60× water-immersion lens.

We thank Jennifer Geiger, Masa Tada and Laurel Rohde for reading earlier versions of this manuscript and Bianca Habermann for generating the phylogenetic tree of *ezrin2*. We are grateful to G. Junghanns, E. Lehmann, M. Fischer and J. Hueckmann for help with the fish care and to S. Witzel and S. Schneider for technical help. This work was supported by the DFG priority program SP 1049 (Molecular Control Mechanisms of Cell Migration) and the EC FP6 Zf-Models project.

References

Adams, J. C. (2004). Roles of fascin in cell adhesion and motility. *Curr. Opin. Cell Biol.* **16**, 590-596.

Barth K. A and Wilson S. W. (1995). Expression of zebrafish nk2.2 is influenced by sonic hedgehog/vertebrate hedgehog-1 and demarcates a zone of neuronal differentiation in the embryonic forebrain. *Development*, **121**, 1755-1768.

Benjamini, Y. and Hochberg, Y. (1995). Controlling the false discovery rate–a practical and powerful approach to multiple testing. *J. R. Stat. Soc. Ser. B Methodol.* **57**, 289-300.

Bretscher, A., Edwards, K. and Fehon, R. G. (2002). ERM proteins and merlin: integrators at the cell cortex. *Nat. Rev. Mol. Cell Biol.* **3**, 586-599.

Crepaldi, T., Gautreau, A., Comoglio, P. M., Louvard, D. and Arpin, M. (1997). Ezrin is an effector of hepatocyte growth factor-mediated migration and morphogenesis in epithelial cells. *J. Cell Biol.* **138**, 423-434.

Dard, N., Louvet, S., Santa-Maria, A., Aghion, J., Martin, M., Mangeat, P. and Maro, B. (2001). In vivo functional analysis of ezrin during mouse blastocyst formation. *Dev. Biol.* **233**, 161-173.

Eisen, M. B., Spellman, P. T., Brown, P. O. and Botstein, D. (1998). Cluster analysis and display of genome-wide expression patterns. *Proc. Natl. Acad. Sci. USA* **95**, 14863-14868.

Feldman, B., Dougan, S. T., Schier, A. F. and Talbot, W. S. (2000). Nodal-related signals establish mesendodermal fate and trunk neural identity in zebrafish. *Curr. Biol.* **10**, 531-534.

Felsenstein, J. (1989). PHYLIP–phylogeny inference package (Version 3.2). *Cladistics* **5**, 164-166.

Gong, L., Puri, M., Unlu, M., Young, M., Robertson, K., Viswanathan, S., Krishnaswamy, A., Dowd, S. R. and Minden, J. S. (2004). Drosophila ventral furrow morphogenesis: a proteomic analysis. *Development* **131**, 643-656.

Gritsman, K., Zhang, J., Cheng, S., Heckscher, E., Talbot, W. S. and Schier, A. F. (1999). The EGF-CFC protein one-eyed pinhead is essential for nodal signaling. *Cell* **97**, 121-132.

Hebestreit, H. F. (2001). Proteomics: an holistic analysis of nature's proteins. *Curr. Opin. Pharmacol.* **1**, 513-520.

Jawhari, A. U., Buda, A., Jenkins, M., Shehzad, K., Sarraf, C., Noda, M., Farthing, M. J., Pignatelli, M. and Adams, J. C. (2003). Fascin, an actin-bundling protein, modulates colonic epithelial cell invasiveness and differentiation in vitro. *Am. J. Pathol.* **162**, 69-80.

Kang, D. H., Gho, Y. S., Suh, M. K. and Kang, C. H. (2002). Highly sensitive and fast protein detection with coomassie brilliant blue in sodium dodecyl sulfate-polyacrylamide gel electrophoresis. *Bull. Korean Chem. Soc.* **23**, 1511-1512.

Kimmel, C. B., Ballard, W. W., Kimmel, S. R., Ullmann, B. and Schilling, T. F. (1995). Stages of embryonic development of the zebrafish. *Dev. Dyn.* **203**, 253-310.

Kureishy, N., Sapountzi, V., Prag, S., Anilkumar, N. and Adams, J. C. (2002). Fascins, and their roles in cell structure and function. *BioEssays* **24**, 350-361.

Lamb, R. F., Ozanne, B. W., Roy, C., McGarry, L., Stipp, C., Mangeat, P. and Jay, D. G. (1997). Essential functions of ezrin in maintenance of cell shape and lamellipodial extension in normal and transformed fibroblasts. *Curr. Biol.* **7**, 682-688.

Link, V., Shevchenko, A. and Heisenberg, C. P. (2006). Proteomics of early zebrafish embryos. *BMC Dev. Biol.* **6**, 1.

Lopez, M. F. (1999). Proteome analysis. I. Gene products are where the biological action is. *J. Chromatogr. B Biomed. Sci. Appl.* **722**, 191-202.

Marlow, F., Topczewski, J., Sepich, D. and Solnica-Krezel, L. (2002). Zebrafish rho kinase 2 acts downstream of wnt11 to mediate cell polarity and effective convergence and extension movements. *Curr. Biol.* **12**, 876-884.

Matsui, T., Maeda, M., Doi, Y., Yonemura, S., Amano, M., Kaibuchi, K., Tsukita, S. and Tsukita, S. (1998). Rho-kinase phosphorylates COOH-terminal threonines of ezrin/radixin/moesin (ERM) proteins and regulates their head-to-tail association. *J. Cell Biol.* **140**, 647-657.

Mhawech, P. (2005). 14-3-3 proteins – an update. *Cell Res.* **15**, 228-236.

Montero, J. A., Kilian, B., Chan, J., Bayliss, P. E. and Heisenberg, C. P. (2003). Phosphoinositide 3-kinase is required for process outgrowth and cell polarization of gastrulating mesendodermal cells. *Curr. Biol.* **13**, 1279-1289.

Montero, J. A., Carvalho, L., Wilsch-Brauninger, M., Kilian, B., Mustafa, C. and Heisenberg, C. P. (2005). Shield formation at the onset of zebrafish gastrulation. *Development* **132**, 1187-1198.

Mullins, M. C., Hammerschmidt, M., Haffter, P. and Nusslein-Volhard, C. (1994). Large-scale mutagenesis in the zebrafish: in search of genes controlling development in a vertebrate. *Curr. Biol.* **4**, 189-202.

Patton, W. F. (1999). Proteome analysis. II. Protein subcellular redistribution: linking physiology to genomics via the proteome and separation technologies involved. *J. Chromatogr. B Biomed. Sci. Appl.* **722**, 203-223.

Puech, P. H., Taubenberger, A., Ulrich, F., Krieg, M., Muller, D. J. and Heisenberg, C. P. (2005). Measuring cell adhesion forces of primary gastrulating cells from zebrafish using atomic force microscopy. *J. Cell Sci.* **118**, 4199-4206.

Rodriguez, L. G. and Guan, J. L. (2005). 14-3-3 regulation of cell spreading and migration requires a functional amphipathic groove. *J. Cell Physiol.* **202**, 285-294.

Rutishauser, U. and Landmesser, L. (1996). Polysialic acid in the vertebrate nervous system: a promoter of plasticity in cell-cell interactions. *Trends Neurosci.* **19**, 422-427.

Sato, N., Funayama, N., Nagafuchi, A., Yonemura, S., Tsukita, S. and Tsukita, S. (1992). A gene family consisting of ezrin, radixin and moesin. Its specific localization at actin filament/plasma membrane association sites. *J. Cell Sci.* **103**, 131-143.

Schier, A. F. (2001). Axis formation and patterning in zebrafish. *Curr. Opin. Genet. Dev.* **11**, 393-404.

Schier, A. F. (2003). Nodal signaling in vertebrate development. *Annu. Rev. Cell Dev. Biol.* **19**, 589-621.

Shevchenko, A., Wilm, M., Vorm, O. and Mann, M. (1996). Mass spectrometric sequencing of proteins silver-stained polyacrylamide gels. *Anal. Chem.* **68**, 850-858.

Solnica-Krezel, L. (2005). Conserved patterns of cell movements during vertebrate gastrulation. *Curr. Biol.* **15**, R213-R228.

Stanford, W. L., Cohn, J. B. and Cordes, S. P. (2001). Gene-trap mutagenesis: past, present and beyond. *Nat. Rev. Genet.* **2**, 756-768.

Stern, C. (2004). *Gastrulation: From Cells to Embryo*. Cold Spring Harbor, NY: Cold Spring Harbor Laboratory Press.

Thompson, J. D., Gibson, T. J., Plewniak, F., Jeanmougin, F. and Higgins, D. G. (1997). The CLUSTAL_X windows interface: flexible strategies for multiple sequence alignment aided by quality analysis tools. *Nucleic Acids Res.* **25**, 4876-4882.

Torres, M. A., Yang-Snyder, J. A., Purcell, S. M., DeMarais, A. A., McGrew, L. L. and Moon, R. T. (1996). Activities of the Wnt-1 class of secreted signaling factors are antagonized by the Wnt-5A class and by a dominant negative cadherin in early Xenopus development. *J. Cell Biol.* **133**, 1123-1137.

Ulrich, F., Krieg, M., Schotz, E. M., Link, V., Castanon, I., Schnabel, V., Taubenberger, A., Mueller, D., Puech, P. H. and Heisenberg, C. P. (2005). Wnt11 functions in gastrulation by controlling cell cohesion through Rab5c and E-Cadherin. *Dev. Cell* **9**, 555-564.

Varki, A. (1997). Sialic acids as ligands in recognition phenomena. *FASEB J.* **11**, 248-255.

Veeman, M. T., Axelrod, J. D. and Moon, R. T. (2003). A second canon. Functions and mechanisms of beta-catenin-independent Wnt signaling. *Dev. Cell* **5**, 367-377.

Wallingford, J. B., Fraser, S. E. and Harland, R. M. (2002). Convergent extension. The molecular control of polarized cell movement during embryonic development. *Dev. Cell* **2**, 695-706.

Warga, R. M. and Kimmel, C. B. (1990). Cell movements during epiboly and gastrulation in zebrafish. *Development* **108**, 569-580.